

Spatial Cross-Correlation Properties of MmWave Massive MIMO Channels

(Invited Paper)

Rui Feng¹, Jie Huang¹, Jian Sun^{1,2}, Yi Tan³, Cheng-Xiang Wang³, and Shidong Zhou⁴

¹Shandong Provincial Key Lab of Wireless Communication Technologies, Shandong University, Jinan, Shandong, 250100, China.

²State Key Lab. of Millimeter Waves, Southeast University, Nanjing, 210096, China.

³Institute of Sensors, Signals and Systems, School of Engineering & Physical Sciences, Heriot-Watt University, Edinburgh, EH14 4AS, U.K.

⁴Department of Electronic Engineering, Tsinghua University, Beijing, 100084, China.

Email: fengxiurui604@163.com, hj_1204@sina.cn, sunjian@sdu.edu.cn, yi.tan@hw.ac.uk, cheng-xiang.wang@hw.ac.uk, zhousd@tsinghua.edu.cn

Abstract—To analyze the propagation characteristics of millimeter wave (mmWave) massive multiple-input multiple-output (MIMO) channels, channel measurements in an office environment using a vector network analyzer (VNA) are carried out. Detailed parameter settings of the measurement system and configuration of the large receiver (Rx) antenna array are introduced. Through dividing the Rx array into several sub-arrays, characteristics like spherical wavefront, non-stationarity, and cluster evolution over the array can be found with parameter estimation using the space alternating generalized expectation-maximization (SAGE) algorithm. For signals received by the virtual horizontal planar array, it is shown that the spatial cross-correlation functions (SCCFs) exhibit significant changes along different dimensions of the Rx horizontal planar array. Thus, it is worth taking the relative angle between transmitter (Tx) pointing direction and Rx array location into consideration while carrying out channel measurements. It is also verified that the SCCFs can be influenced by the measurement environment, the coordinates of antenna elements in the large array, as well as the operated frequencies.

Index Terms—Massive MIMO, millimeter wave, 5G, planar array, spatial cross-correlation function.

I. INTRODUCTION

Increasing demands of high capacity, energy efficiency, spectral efficiency, and reliability have expedited the research of the fifth generation (5G) communication systems. New technologies such as mmWave and massive MIMO have been proposed and widely studied to enable a dramatic improvement of channel capacity and spectrum limitation [1]. The combination of several techniques also has significant contribution to the system performance [2]. For example, mmWave and massive MIMO can be complement regarding the antenna array size and cell coverage.

MmWave massive MIMO channels show some new characteristics and researchers have carried out many channel measurements to study the propagation channel characteristics. It was introduced in [3] that, massive MIMO channels exhibited characteristics such as spherical wavefront and spatial non-stationarity as the array size is much larger than conventional MIMO channels. Power imbalance on the antenna array and statistical properties like spatial-temporal-frequency correla-

tion function (STFCF) were investigated. Lund University conducted many massive MIMO channel measurements using 128-element uniform linear array (ULA) and cylindrical array, respectively. The sum-rate capacity and condition number to separate closely spaced users were investigated [4], and it was pointed out that the non-stationarity and near field effect can help decorrelating channels for different users [5]. In [6], channel measurements carried out at four mmWave frequency bands with large uniform virtual planar arrays were introduced to validate the spherical wavefront, cluster birth-death, and non-stationarity properties. In this paper, we divide the large antenna array into several sub-arrays and extract channel parameters for each sub-array using the SAGE algorithm. Thus, those characteristics can be simply validated by analyzing the estimated parameters.

However, we find that channel statistical properties like SCCFs in different dimension of a planar array have never been analyzed or compared before. This paper focuses on the discussion of SCCFs along two distinct dimensions of a horizontal large planar array and impacts of Tx locations and the operated mmWave frequencies on spatial correlation properties. We find that SCCF is not only a very useful term to check the correctness of measurement data, but also able to show how the channel properties change at different antenna positions and frequency bands. The correlation coefficient is verified to be affected by the measurement environment, operated frequency, relative locations of Tx and Rx, and the angle between the Tx pointing direction and Rx array. Furthermore, the difference of SCCFs along different dimensions of the large array should be taken into consideration while proposing massive MIMO channel models.

The remainder of this paper is organized as follows. The signal model is introduced in Section II. Channel measurement environment and system setups are described in Section III. In Section IV, the measurement results are given and the SCCFs are analyzed. Finally, conclusions are drawn in Section V.

II. SIGNAL MODEL

In a time invariant near-field scenario, multipath components (MPCs) impinging at the Rx array element have different complex amplitudes, delays, and angle of arrivals (AoAs). The channel impulse response (CIR) can be expressed by summing L MPCs up [7],

$$h(t; \alpha, \tau, \Omega_R) = \sum_{l=1}^L \alpha_l u(t - \tau_l) \mathbf{c}(\Omega_R - \Omega_{R,l}) + \sqrt{\frac{N_0}{2}} N(t) \quad (1)$$

where $u(t)$ is the transmitted signal, α_l , τ_l , and $\Omega_{R,l}$ are the complex amplitude, delay, and AoA of the l -th path, respectively. $N(t)$ is the complex white Gaussian noise with unit spectral height N_0 . Steering vector $\mathbf{c}(\Omega_R)$ represents the response of the Rx array to a wave coming from direction Ω_R , which can be expressed as [7]

$$\mathbf{c}(\Omega_R) = \exp\{j2\pi\lambda^{-1} \langle e(\Omega_R), r_R \rangle\} \quad (2)$$

with λ and r_R denote the wavelength and antenna location vector, and $e(\Omega_R)$ is the unit vector in the spherical coordinates.

We assume a horizontal planar Rx array consists of $M \times N$ antennas, and let $h_{m,n}$ and $h_{m',n'}$ denote the measured CIRs at the Rx antenna element with coordinates (m, n) and (m', n') in the x - y plane, respectively. The correlation coefficient between $h_{m,n}$ and $h_{m',n'}$ can be given as

$$\rho_{h_{m,n}, h_{m',n'}} = \frac{E\{(h_{m,n} - \bar{h}_{m,n})(h_{m',n'} - \bar{h}_{m',n'})\}}{\sqrt{E\{(h_{m,n} - \bar{h}_{m,n})^2(h_{m',n'} - \bar{h}_{m',n'})^2\}}} \quad (3)$$

where $E\{\cdot\}$ denotes the expectation considering K delay bins, $\bar{h}_{m,n}$ and $\bar{h}_{m',n'}$ are the mean values of CIRs. The correlation distance is usually defined as the antenna distance where the spatial correlation coefficient decreases to 0.5.

III. MMWAVE MASSIVE MIMO CHANNEL MEASUREMENTS

A. Measurement Environment and Setup

To study the propagation channel characteristics in indoor mmWave massive MIMO channels, channel measurements in an office using the Keysight N5227A VNA are conducted. As shown in Fig. 1, the office is furnished with multiple chairs, desks, computers, and electronic devices. Tx and Rx are connected to Port 1 and Port 2 of the VNA through cables, respectively. The size of the office is $7.2 \times 7.2 \times 3$ m 3 . The locations of Tx1, Tx2, and Rx array center are $(2.2, 4, 2.6)$, $(3, 3.6, 2.6)$, and $(3, 1, 1.45)$, respectively. Close to the Rx, a whiteboard with an area of 1.5 m 2 is vertically placed. During channel measurements, the environment is kept quasi-static. During the measurement, the environment is kept quasi-static. To compare the channel characteristics at different mmWave frequency bands, we conduct measurements at 11 and 38 GHz. Detailed system setups can be found in Table I, and the antenna array configurations are described in Section III, B.

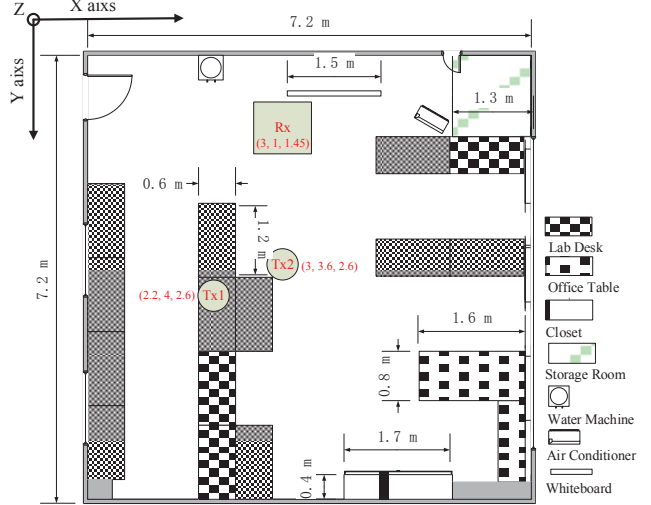


Fig. 1. Layout of the indoor office.

TABLE I
MEASUREMENT SETTINGS.

Center frequency, f (GHz)	11	38
Wavelength, λ (mm)	27	8
Bandwidth, B (GHz)	2	4
Output power, P (dBm)	15	8
Sweeping points, K	401	801
Rx array elements	51×51	121×121
Array size (mm 2)	600×600	360×360
Antenna spacing step, $d_x = d_y$ (mm)	12	3
Rayleigh distance, R (m)	53.3	64.8

B. Antenna Array Configurations

During the measurement, a 10 dBi horn antenna is placed at two Tx locations successively, while the Rx omnidirectional antenna working at 3–40 GHz bands is placed on a positioner to shift positions, thus to form a massive virtual horizontal uniform planar array. Tx is aligned to the center of the large Rx array.

In order to have a vivid exhibition of the configurations of Tx and Rx, a simplified geometrical structure of the office room, two Tx locations, and Rx array are shown in Fig. 2. Specific places of the Rx antenna elements can be symbolized by the x' - y' - z' coordinates. It is also clear to see that the distances of Tx1 and Tx2 to Rx are 3.3 m and 2.8 m, respectively.

IV. MEASUREMENT RESULTS AND ANALYSIS

A. Data Processing Using the SAGE Algorithm

In this section, we analyze the measurement data received at Tx2 in 38 GHz. Considering that the Rayleigh distance for the whole array is beyond the office dimensions, the Rx array is divided into several sub-arrays with antenna elements equal

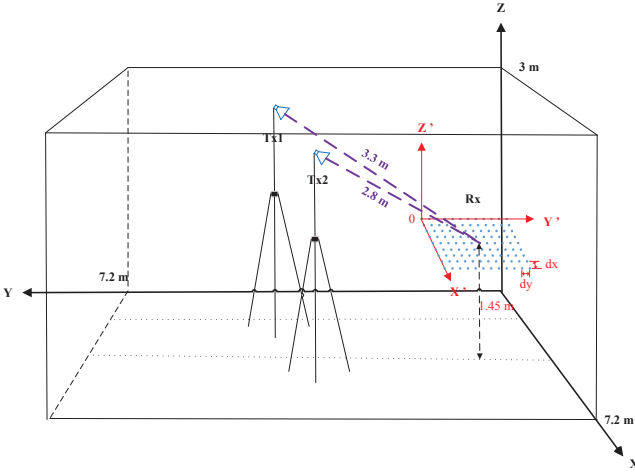


Fig. 2. Tx and Rx antenna array configurations.

to 20×20 . Thus, we can see how the parameters of MPCs variate over the sub-array by using the SAGE algorithm. In this paper, we select sub-arrays 1 and 2, as shown in Fig. 3, to analyze the parameter variations.

We use the SAGE algorithm to extract 100 MPCs for each sub-array, and check the correctness of the estimated results by comparing with the measured power delay profiles (PDPs). Also, we can verify the correctness of estimated azimuth angles of arrival (AAoAs) by finding the possible travel paths. As shown in Fig. 4, the measured and estimated PDPs of the sub-array 1 are plotted. Typical line of sight (LoS) components with delays around 9.25 ns are extracted, which corresponds to the travelling time from Tx to Rx sub-array 1. Other reflected and scattered MPCs with smaller powers are also estimated accurately referring to the measurement data.

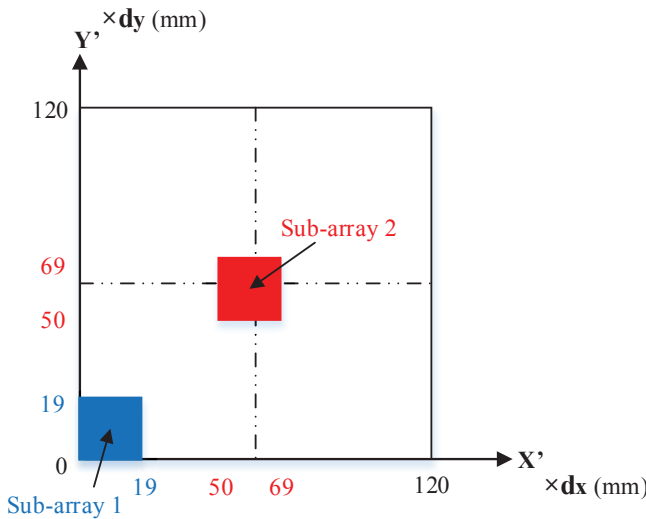


Fig. 3. Two selected sub-arrays in the Rx array.

As Rx is a horizontal array, we cannot distinguish signals from up and below, so elevation angles of arrival (EAoAs) are not studied in this paper, though it is important in the indoor near-field scenario. In order to see how the AAoAs and powers variate at different antenna elements of the large array, the power angular profiles (PAPs) for sub-arrays 1 and 2 are compared in Fig. 5 with dynamic range of 30 dB. The LoS components for sub-array 2 have power up to -69 dB and AAoA equals to 16° , while the power is -73 dB and AAoA equals to 13° for sub-array 1. Thus, the variation of power is unneglectable, which shows the non-stationarity of massive MIMO channel. The shift of AAoAs for LoS components verifies the importance of considering antenna element location within the Rx array. Another phenomenon that cannot be neglected is that sub-arrays 1 and 2 can see different scatterers. For example, for sub-array 1, MPC with AAoA equals to 176° is not captured by sub-array 2. That means the cluster evolution along the array should also be taken into account.

B. Comparison of SCCFs Along Different Dimensions of the Planar Array

In order to see how the channel changes along different dimension of the horizontal planar array, we firstly select the measurement data of one virtual ULA from the planar array to calculate the spatial correlation coefficients towards the positive direction of the x' axis. The selected ULA lies in line with $y' = 26$ which is parallel to the x' axis and cut the planar array into half. In Fig. 6(a), the SCCFs calculated according to (3) from 11 GHz channel measurement data at Tx1 and Tx2 are shown. It can be seen that, correlation coefficients of Tx2 along x' axis are all above 0.8, while those of Tx1 are smaller than that of Tx2 but still larger than 0.5. That means signals received by the linear antenna array along x' axis are highly correlated, even when the antenna spacing distance is extended to 600 mm.

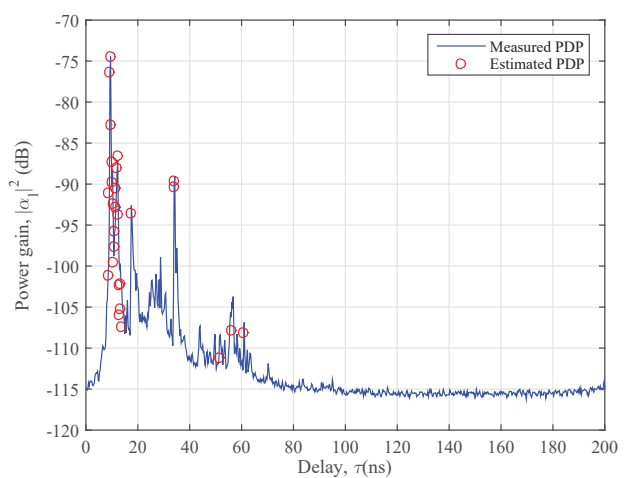


Fig. 4. Measured and estimated PDPs.

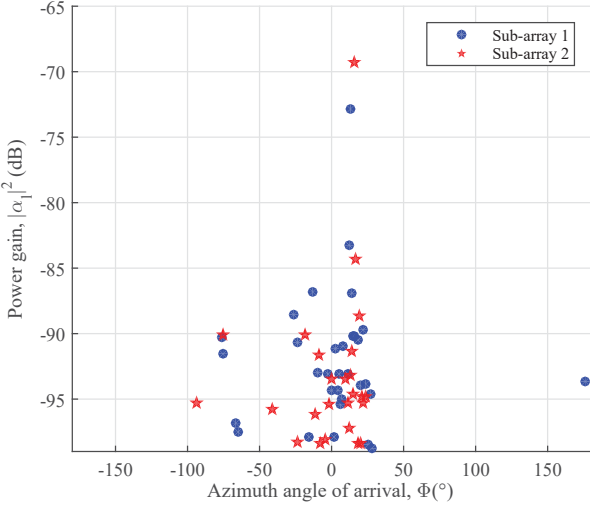


Fig. 5. Estimated PAPs of two sub-arrays.

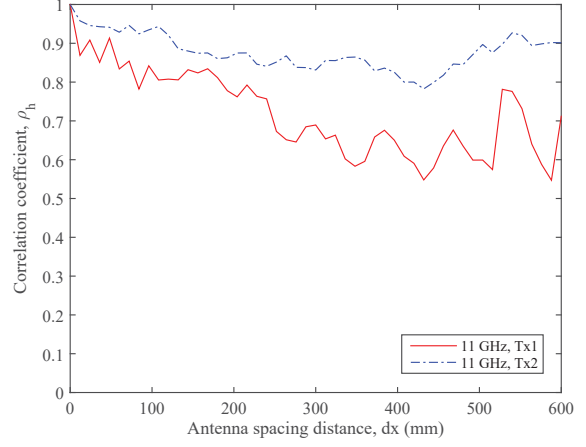
Similarly, we select the ULA lying in line $x' = 26$ to calculate the spatial correlation coefficients towards the positive direction of the y' axis. SCCFs shown in Fig. 6(b) are calculated from measurement data at Tx1 and Tx2, respectively. It is obvious to see the difference with that in Fig. 6(a), as these two curves are decreased to approximate 0. It can be interpreted by the increasing distance between Tx and antenna element along the y' axis. However, SCCF calculated for Tx2 exhibits a valley shape and the coefficients increase when antenna spacing distance larger than 300 mm, this is caused by the reason that Tx2 is aligned to the center of the extracted ULA.

C. Variations of Channel Correlation Properties at Different Frequency Bands

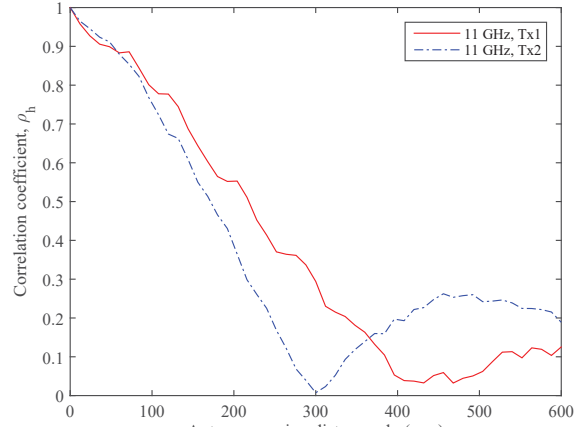
We choose antenna elements located in x' and y' axes as base points to calculate SCCFs along y' and x' axes and combine those curves together, respectively, as shown in Fig. 7. Thus, a comprehensive exhibition of how the channel correlation properties change along x' and y' axes are obtained. Fig. 7 is plotted based on measurement data of Tx1 at 11 and 38 GHz frequency bands.

As shown in Fig. 7(a) and (c), SCCFs along the x' axis at 38 GHz decrease fast and the correlation coefficients reach 0.2, while at 11 GHz the correlation coefficients still above 0.3 and even larger than 0.6. The same tendency of how the SCCFs change when channel moves to higher mmWave frequency band can be seen when comparing Fig. 7(b) with Fig. 7(d). This is caused by the more abundant scattering components at higher mmWave frequency band. However, SCCF curves plotted in Fig. 7(b) and (d) are very much different with those in Fig. 7(a) and (c), as introduced in Section IV, B.

Thus, we conclude that distance between Tx and Rx elements and operated frequency have impacts on the propagation



(a)



(b)

Fig. 6. Measured SCCFs at Tx1 and Tx2 (a) along x' -axis and (b) along y' -axis.

channel characteristics. It is also worth taking the relative angle between Tx pointing direction and Rx array into consideration, as the calculated SCCFs along two certain directions exhibit significant variations.

V. CONCLUSIONS

In this paper, channel measurements at 11 and 38 GHz frequency bands have been carried out at two different locations in a typical indoor environment. Detailed measurement environment, system setup, and massive antenna array settings have been introduced. Parameters of MPCs estimated using the SAGE algorithm and spatial cross-correlation properties calculated for the large horizontal planar array have been investigated. Through comparing the parameters of two sub-arrays, new characteristics of massive MIMO channels have been introduced. Variations of the SCCFs at two distinct directions of the horizontal massive array have been shown by calculating the spatial correlation coefficients of the selected ULAs, and compared at different Tx locations and frequency

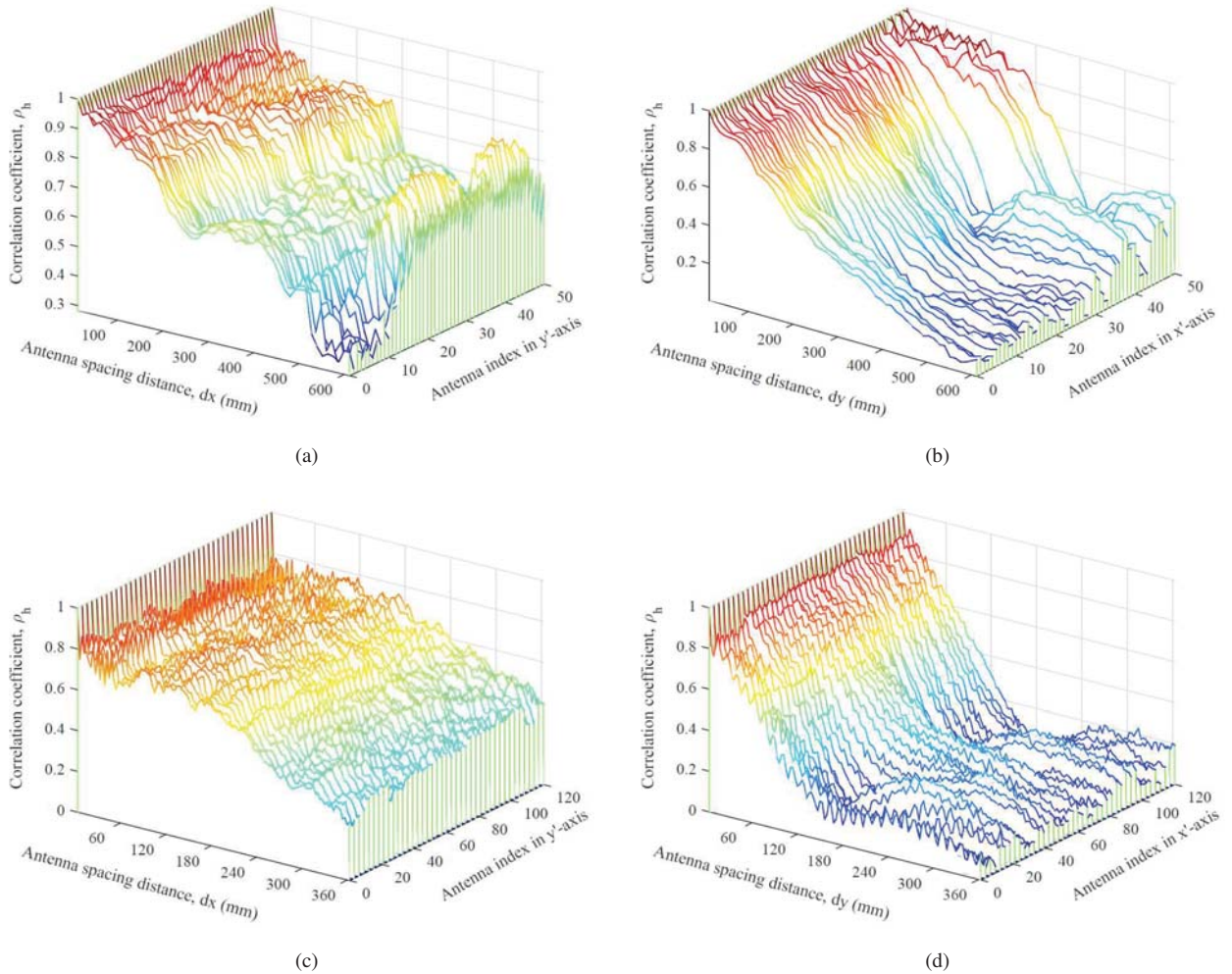


Fig. 7. Measured SCCFs at Tx1 (a) along x' -axis, 11 GHz; (b) along y' -axis, 11 GHz; (c) along x' -axis, 38 GHz; (d) along y' -axis, 38 GHz.

bands. Results have shown that, measurement environment, relative distance of Tx and Rx, certain positions of antenna elements, as well as the operated frequencies have significant impacts on the space cross-correlation properties.

ACKNOWLEDGMENT

The authors would like to acknowledge the support from Natural Science Foundation of China (No. 61771293, 61371110), Fundamental Research Funds of Shandong University (No. 2017JC029), Key R&D Program of Shandong Province (No. 2016GGX101014), EPSRC TOUCAN project (No. EP/L020009/1), and EU H2020 RISE TESTBED project (No. 734325).

REFERENCES

- [1] C.-X. Wang, F. Haider, X. Gao, X.-H. You, Y. Yang, D. Yuan, H. Aggoune, H. Haas, S. Fletcher, and E. Hepsaydir, "Cellular architecture and key technologies for 5G wireless communication networks," *IEEE Commun. Mag.*, vol. 52, no. 2, pp. 122–130, Feb. 2014.
- [2] A. L. Swindlehurst, E. Ayanoglu, P. Heydari, and F. Capolino, "Millimeter-wave massive MIMO: The next wireless revolution?" *IEEE Commun. Mag.*, vol. 52, no. 9, pp. 56–62, Sept. 2014.
- [3] S. Wu, C.-X. Wang, H. Haas, H. Aggoune, M. M. Alwakeel, and B. Ai, "A non-stationary wideband channel model for massive MIMO communication systems," *IEEE Trans. Wireless Commun.*, vol. 14, no. 3, pp. 1434–1446, Mar. 2015.
- [4] X. Gao, O. Edfors, F. Rusek, and F. Tufvesson, "Massive MIMO performance evaluation based on measured propagation data," *IEEE Trans. Wireless Commun.*, vol. 14, no. 7, pp. 3899–3911, Jul. 2015.
- [5] S. Payami, and F. Tufvesson, "Channel measurements and analysis for very large array systems at 2.6 GHz," in *Proc. EuCAP'12*, Prague, Czech Republic, Mar. 2012, pp. 433–437.
- [6] J. Huang, C.-X. Wang, R. Feng, J. Sun, W. Zhang, and Y. Yang, "Multi-frequency mmWave massive MIMO channel measurements and characterization for 5G wireless communication systems," *IEEE J. Sel. Areas Commun.*, 2017, accepted for publication.
- [7] B. H. Fleury, M. Tschudin, R. Heddergott, D. Dahlhaus, and K. I. Pedersen, "Channel parameter estimation in mobile radio environments using the SAGE algorithm," *IEEE J. Sel. Areas Commun.*, vol. 17, no. 3, pp. 434–450, Mar. 1999.